26 May 2010, 2:45 pm - 3:30 pm

Case Histories and Energy-Based Evaluation on Travel Distance of Slope Failures During Recent Earthquakes

Takaji Kokusho
Chuo University, Japan

Tomohiro Ishizawa
Chuo University, Japan


Fifth International Conference on
Recent Advances in Geotechnical Earthquake Engineering and Soil Dynamics
and Symposium in Honor of Professor I.M. Idriss
May 24-29, 2010 • San Diego, California

CASE HISTORIES AND ENERGY-BASED EVALUATION ON TRAVEL DISTANCE OF SLOPE FAILURES DURING RECENT EARTHQUAKES

Takaji Kokusho
Chuo University
Faculty of Science & Engineering
Tokyo, Japan.

Tomohiro Ishizawa
Chuo University
Faculty of Science & Engineering
Tokyo, Japan.

ABSTRACT

An energy approach evaluating travel distance of debris in slope failures is proposed here, in which earthquake energy and gravitational potential energy are dissipated in flow deformations. Shake table model tests of dry sand slopes are carried out in which the earthquake energy dissipated in slope failure can be successfully quantified. The model tests indicate that measured slope displacements can be reliably evaluated by the proposed energy approach based on a rigid block model if an appropriate friction coefficient of the slope is specified. The energy approach is then applied to a number of slopes failed during recent earthquake in Japan to back-calculate mobilized friction coefficients, revealing their strong dependency on initial slope inclinations. It is clarified that the earthquake energy is actually much smaller than the potential energy for most of large slides, though it plays an important role of triggering slides. The friction coefficients are found smaller than the initial slope inclinations for gentler slopes, indicating that the failed soil masses tend to accelerate during sliding. The friction coefficients tend to decrease with increasing volume of failed slopes, which is compatible with previous case studies including large non-seismic landslides.

INTRODUCTION

Seismically induced slope failures have normally been evaluated based on force equilibrium on a potentially sliding soil mass. This force approach can evaluate a safety factor against slope failure, but cannot predict slide deformation, once failure occurs. From a viewpoint of performance based design or risk evaluation of slope failures, it is important to know not only the safety factor but also how large deformation develops and how far failed soil mass reaches down-slope. The Newmark method (Newmark 1965) or its modifications by using FEM analyses (e.g. Makdisi and Seed 1978) can evaluate displacement of a rigid soil block along a fixed slip surface based on a double integration of acceleration acting on it. In actual slope failures, however, sliding soil may not necessarily behave as a rigid body but deforms continuously with movable slip surfaces. It sometimes tends to become destructive due to a shift from slow rigid-block slide to fast debris flow because the friction coefficient decreases drastically after the initiation of failure.

In order to evaluate slope failures including flow failures from their initiation to termination, an energy approach was first proposed by Kokusho and Kabasawa (2003) and further developed by Kokusho and Ishizawa (2007). In that method, four energies; potential energy change by the gravity $-\delta E_p$, earthquake energy contributing to slope failure E_{EQ}, dissipated energy in a sliding soil mass E_{DP}, and kinetic energy E_k of the sliding soil mass are correlated by the following equation;

$$-\delta E_p + E_{EQ} = E_{DP} + E_k \quad (1)$$

or in an incremental form as;

$$-\Delta\delta E_p + \Delta E_{EQ} = \Delta E_{DP} + \Delta E_k \quad (2)$$

Note that the potential energy change before and after failure δE_p in Eq.(1) or $\triangle\delta E_p$ in Eq.(2) is normally negative.

Once failure starts, the amount of the dissipated energy in debris is critical to decide if it develops as a flow-type failure and how far it flows. In time increments when earthquake shaking has already ended, ($\triangle E_{EQ}$ =0 or $-\triangle\delta E_p = \triangle E_{DP} + \triangle E_k$), if $\triangle E_{DP}$ is smaller than $-\triangle\delta E_p$, then $\triangle E_k$ is positive and the soil mass accelerates. It may also be inferred that a shift from slow slide to fast flow may occur not only due to an increase in $-\triangle\delta E_p$ but also due to a drastic decrease of $\triangle E_{DP}$ caused by pore-pressure buildup in liquefiable soil, strength loss in high-sensitivity clay, etc. In fast flow failures, soil mass will keep flowing unless the kinetic energy plus the subsequent potential energy change is all dissipated in the sliding soil mass. Namely, if $-\triangle\delta E_p$ is smaller than $\triangle E_{DP}$, then $\triangle E_k$ is negative, hence the soil mass decreases the speed and comes to a halt when the reserved kinetic energy E_k is all consumed. Thus, provided that the earthquake energy and the energy dissipation mechanism in flowing soil mass are known, it is possible to evaluate the run-out distance in flow-type slides by the energy approach.

In this paper, a series of model tests are first addressed to discuss on the energy balance in a model slope made from dry sand. The test results are then compared with a simple Newmark-type rigid block model to develop an evaluation method for slope deformation based on the energy concept. The energy-based simple evaluation method is then applied to a number of slopes failed during recent earthquakes to back-calculate mobilized friction coefficients and discuss on how the friction coefficients are determined according to various parameters of slopes.

SHAKE TABLE TEST

A spring-supported shaking table shown in Fig. 1(a) was utilized to test a model slope made from dry sand, called Model-A here, in a rectangular lucite box of 80 cm in length, 50 cm in height and 40 cm in width. The slope angle was parametrically changed as 29, 20 and 10 degrees, considering the angle of repose of the same model slope (35.4 degree). The table was initially pulled to several different horizontal displacements and then released to generate decayed free vibration. The frequency of the vibration was changed in 4 steps, from 2.7 Hz to 2.5, 2.2 and 2.0 Hz by attaching 1 to 3 additional steel plates of the same mass to the table.

Dissipated energy, which can be calculated from displacement amplitudes in the decay vibration depends not only on the energy dissipation due to slope failure but also on other energy loss mechanisms such as radiation into the shake table foundation, friction in the springs, etc. In order to single out the dissipated energy due to slope deformation, not only Model-A but Model-B, a pile of rigid concrete columns of exactly the same weight, was tested in the same lucite box in the same way (See Fig. 1(b)). The concrete columns were fixed to the box by clamps not to allow energy dissipation due to their relative movements.

The decay in amplitudes, measured by a LVDT displacement gauge in both Model-A and B are exemplified in Fig. 2. Note that the difference in amplitudes grows larger with the number of cycles, though the initial table displacement and the vibration period of the table are almost the same between the two models. It may be reasonable to assume that this difference reflects the greater energy dissipated in Model-A (the model slope) due to its deformations than in Model-B. The earthquake energy increment dissipated in the model slope $\triangle E_{EQ}$ in Eq.(2) is evaluated from the loss energy per cycle in Model-A $\triangle W_A$,and that in Model-B, $\triangle W_B$ as $\triangle E_{EQ} = \triangle W_A - \triangle W_B$, because the loss energy in the two models can be assumed identical except that dissipated inside the

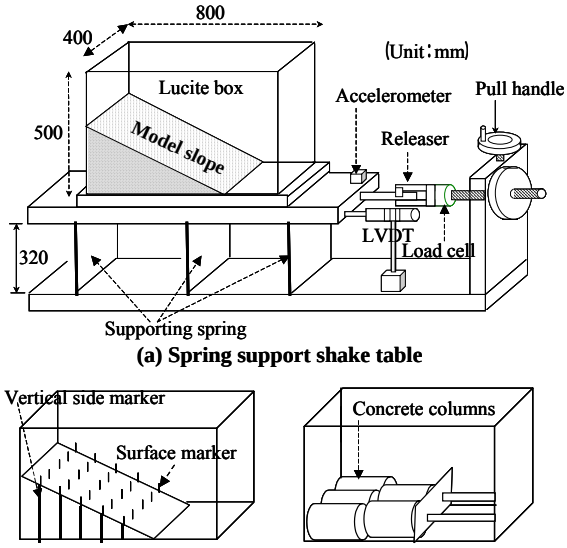

Fig.1 Shake table test apparatus for model slopes (a) and 2 models compared (b).

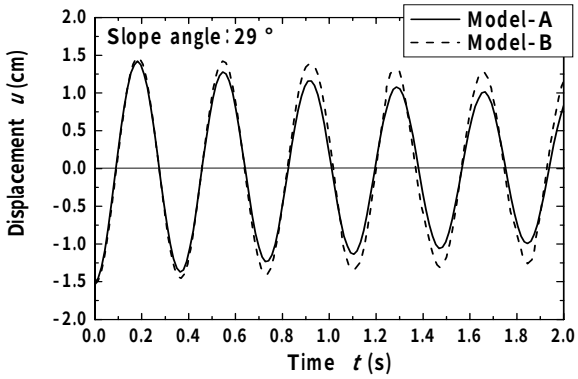

Fig.2 Decay vibrations measured by displacement gauge in Model-A and B.

sand slope. The total energy E_{EQ} calculated as a sum of $\triangle E_{EQ}$ in each cycle represents the amount of earthquake energy involved in producing the residual displacement in the model slope.

In order to correlate the energies with the residual displacement of the slope, horizontal displacement δ_{rs} of the slope was quantified from the video images. Details on definition and measurement of slope displacement are available in other literature (Kokusho and Ishizawa 2007). The incremental potential energy $-\triangle\delta E_p$ is calculated also from the slope surface geometry in the video images as;

$$\triangle\delta E_p = \triangle\left(\rho g B \int z dx dz\right) \tag{3}$$

where ρ = the soil density (assumed constant), g = acceleration of gravity, and B = thickness of the 2-dimensional model. Coordinates x and z are in horizontal and vertical directions of the slope and the integration in terms of x and z is carried out over the cross-sectional area of the slope. The incremental energies, $\triangle E_{EQ}$ and $-\triangle\delta E_p$, calculated in each cycle are summed up to evaluate the corresponding total energies, E_{EQ} and $-\delta E_p$. Then, the dissipated energy E_{DP} can be readily evaluated from Eq.(1) in which E_k=0 if the energy balance after the end of slope failure is concerned. The total residual displacement δ_{rs} is also calculated by summing up all incremental displacements $\triangle\delta_{rs}$.

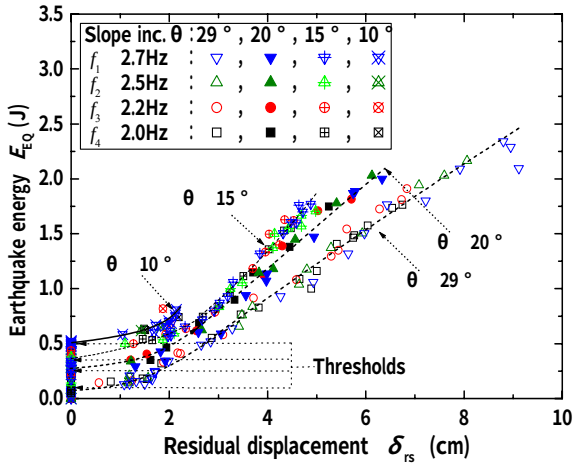

Fig. 3 Residual slope displacements δ_{rs} versus vibration energy E_{EQ} for 4 different slope angles under 4 different input frequencies

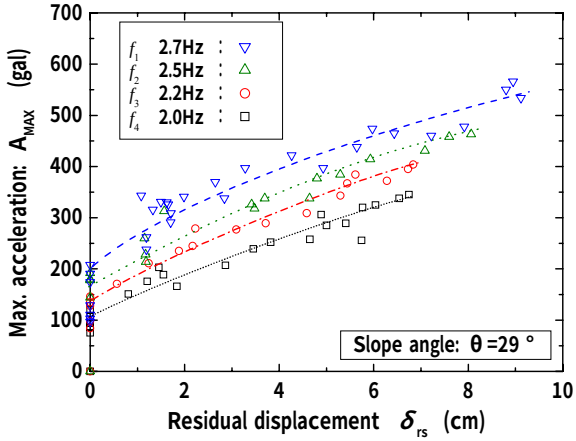

Fig. 4 Residual slope displacements δ_{rs} versus maximum acceleration A_{max} for 4 different slope angles under 4 different input frequencies

In Fig. 3 the residual displacements δ_{rs} are plotted versus the vibration energy E_{EQ} contributed to slope deformations for 4 different slope angles of 29, 20, 15 and 10 degrees under 4 different input frequencies. It is remarkable that, for each slope angle, all plots can be approximated as a single curve, indicating that the energy can serve as a unique determinant for slope displacement even under different shaking frequencies. In addition to the free decay vibration tests, forced vibration tests, which are more analogous to earthquake shaking, were also implemented, which gave almost the same results as free vibration tests previously done, demonstrating the relevance of the energy concept to slope failure mechanism (Kokusho et al. 2009a).

As obviously seen in Fig. 3, the gentler the slope is, the greater is the energy E_{EQ} to attain the same residual displacement δ_{rs}. Also noted in Fig. 3 is that there seems to exist a threshold energy, corresponding to each slope angle, below which no residual displacement occurs, indicating that the energy determines not only residual displacements but also the initiation of slope failure. In order to emphasize the uniqueness of the displacement versus energy relationship, the same residual displacement data of the 29 degrees slope are plotted versus maximum accelerations $A_{\max}$ in place of the energy in Fig. 4, respectively. Here, $A_{\max}$ represents the acceleration in the first cycle of the decayed free vibration. Obviously, the same acceleration results in different residual displacements under different input frequencies despite some data scatters, indicating that acceleration cannot be a unique determinant for slope failure not only for the residual slope displacement but even for the initiation of failure.

DATA INTERPRETATION BY RIGID BLOCK MODEL

A Newmark-type rigid block model was examined from the viewpoint of energy by Kokusho and Ishizawa (2007). The application of the energy approach to the rigid block shown in Fig. 5(a) gives the potential energy change $-\delta E_p$ and the dissipated energy due to the block slippage E_{DP} to be correlated with horizontal residual displacement δ_r as;

$$-\delta E_p = \beta M g \delta_r \tag{4}$$

$$E_{DP} = \frac{\mu\left(1+\beta^2\right)}{1+\mu\beta} M g \delta_r \tag{5}$$

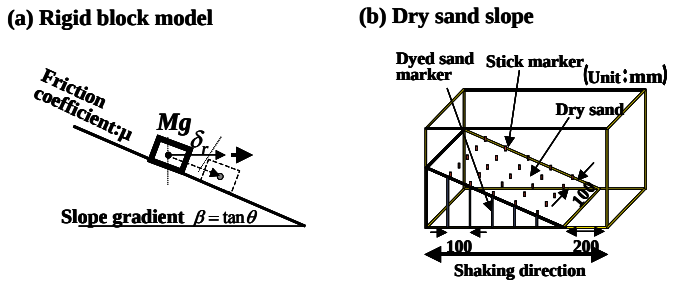

Fig.5 Comparison of models of rigid block and dry sand

where M = mass of sliding soil block, $\beta = \tan\theta$ (θ = slope angle) is slope inclination and $\mu = \tan\phi$ (ϕ = friction angle) is friction coefficient.

Then, starting from Eq.(1) and using $E_k = 0$ if compared before and after slope failure, the earthquake energy is correlated with δ_r as;

$$E_{EQ} = -\left(-\delta E_p\right) + E_{DP} = \frac{\mu-\beta}{1+\mu\beta} Mg\delta_r \qquad (6)$$

The ratios of E_{EQ} to $-\delta E_p$ is;

$$\frac{E_{EQ}}{-\delta E_p} = \frac{(\mu-\beta)}{\beta(1+\mu\beta)} \qquad (7)$$

Note that the contribution of the earthquake energy in comparison to the potential energy depends only on β and μ. Also note that the contribution of E_{EQ} becomes larger than $-\delta E_p$ with decreasing slope inclination β (Kokusho and Ishizawa 2007).

In these relationships, dynamic changes of seismic inertia force affect not only the driving force of the sliding block but also the shear resistance along the slip surface. If the slip plane is saturated, however, it should be assumed that the seismic inertia force is all carried by temporary pore-water pressure and does not change the effective stress normal to the plane, and hence the shear resistance. In this case, it is easy to understand that the dissipated energy E_{DP} can be expressed as the shear resistance along the slip plane, $\mu\sigma'_{n0}\left(1+\beta^2\right)^{1/2} A$, multiplied by the displacement along the slip plane, $\left(1+\beta^2\right)^{1/2}\delta_r$, where σ'_{n0} is effective stress normal to the plane and A is the horizontal area of the sliding soil mass.

Consequently, for saturated slip plane, Eqs.(4) and (5) are replaced by Eqs.(4') and (5'), in which $\sigma_{n0} = Mg \Big/ \left[\left(1+\beta^2\right)A\right]$ is the total stress normal to the slip plane, σ'_{n0} is the corresponding effective stress and A is the horizontal area of the sliding soil mass (Kokusho and Ishizawa 2007).

$$-\delta E_p = \beta\sigma_{n0}\delta_r A\left(1+\beta^2\right) \qquad (4')$$

$$E_{DP} = \mu\sigma'_{n0}\delta_r A\left(1+\beta^2\right) \qquad (5')$$

Then, Eq.(6') is obtained in place of Eq.(6).

$$E_{EQ} = \left(\mu\sigma'_{n0} - \beta\sigma_{n0}\right)\left(1+\beta^2\right)A\delta_r = \left(\mu\frac{\sigma'_{n0}}{\sigma_{n0}} - \beta\right)Mg\delta_r \qquad (6')$$

The energy ratio; Eq.(7), are replaced by Eq.(7') accordingly.

$$\frac{E_{EQ}}{-\delta E_p} = \frac{\mu\sigma'_{n0} - \beta\sigma_{n0}}{\beta\sigma_{n0}} = \frac{\left(\sigma'_{n0}/\sigma_{n0}\right)\mu - \beta}{\beta} \qquad (7')$$

From Eqs.(6) and (6'), the residual slope displacement for the rigid block model can be formulated for the unsaturated case as;

$$\delta_r = \frac{1+\mu\beta}{\mu-\beta}\frac{E_{EQ}}{Mg} \qquad (8)$$

and for the saturated case as;

$$\delta_r = \frac{1}{\mu\left(\sigma'_{n0}/\sigma_{n0}\right) - \beta}\frac{E_{EQ}}{Mg} \qquad (8')$$

In Fig. 6, the residual displacements δ_{rs} (considered here to be equivalent to δ_r in the rigid block model) obtained by a number of tests for different slope angles and different input frequencies are plotted versus the normalized earthquake energies E_{EQ}/Mg. The weight of the displaced soil mass Mg was evaluated from Eq.(4) using the measured potential energy $-\delta E_p$ and the measured displacement δ_{rs} to comply with the rigid block theory.

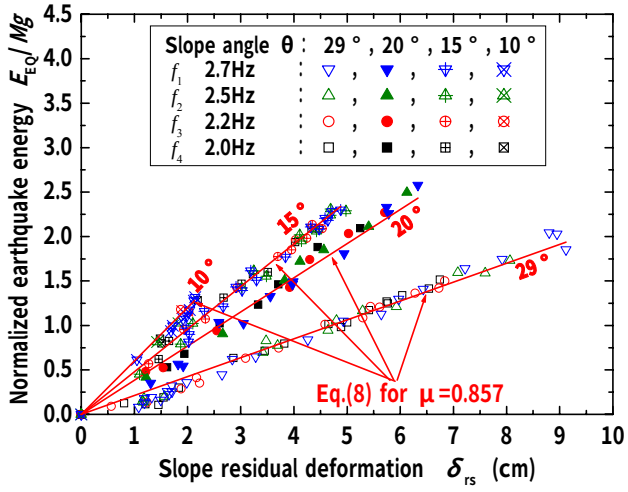

Fig. 6. Earthquake energy versus residual slope displacement for different slope angles by different input frequencies obtained by shake table tests.

It is remarkable that if μ =0.857 is chosen, Eq.(8) can predict the residual slope displacement almost perfectly for all slope angles and all input frequencies. This indicates that if an appropriate friction coefficient is known in advance, the simple rigid block model shown in Fig. 5(a), which apparently involves the failure mechanism quite different from the sand slope in Fig. 5(b), can successfully simulate the realistic failure.

EVALUATION METHOD FOR RUNOUT DISTANCE

Based on the model test results and their interpretation in terms of the rigid block theory, an energy-based evaluation method for run-out distance of earthquake-induced slope failure is proposed. First, the sloping ground is idealized as an equivalent horizontal 2-layer system consisting of an upper layer, which includes the slope, and a base layer (Kokusho and Ishizawa 2007). The input energy transmitting upward through a unit horizontal area, E_{IP}/A, can be formulated (Kokusho et al. 2007) as:

$$E_{IP}/A = \rho Vs \int (\dot{u})^2 dt \qquad (9)$$

where $\dot{u}$ is particle velocity of a wave propagating upward in a base layer, and ρVs is the impedance of the layer (ρ = soil density and Vs = S-wave velocity).

Fig. 7 shows the incident wave energies plotted versus hypocentral distances on a log-log diagram obtained by separate researches (Kokusho 2009) based on vertical array seismic records during recent strong earthquakes in Japan (1995 Kobe EQ., 2003 Tokachi-Oki EQ., 2004 Niigataken Chuetsu EQ. and the 2007 Niigataken Chuetsu-Oki EQ.). It indicates that the input energy per unit horizontal area, E_{IP}/A, evaluated by Eq.(9) in a base layer of about 100-300 m deep can be approximated by the straight lines representing Eq.(10)

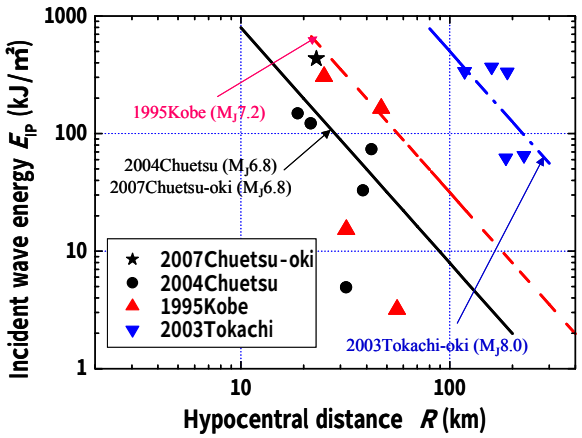

Fig. 7. Incident seismic wave energy versus hypocentral distance calculated from vertical array records, compared to a simple theory of spherical energy radiation.

$$E_{IP}/A = E_0 \Big/ \left(4\pi R^2\right) \qquad (10)$$

where R is the hypocenter distance, and E_0 is the total wave energy in the unit erg (1 erg = 10^{-10} kJ), which is assumed to radiate from the hypocenter. The energy E_0 is determined using the empirical equation by Gutenberg (1955)

$$\log E_0 = 1.5M + 11.8 \qquad (11)$$

where M is the earthquake magnitude using the Richter scale (Note: The Japanese Earthquake Magnitude, M_J, was used here to compute E_0 because the Richter and Japanese magnitude scales are almost equivalent). Data points for the calculated energy from the vertical array records at base layers were found mostly consistent with Eqs.(10) and (11), despite simple assumptions in the energy evaluation without characterizing fault mechanisms such as fault dimension, directivity, asperity, etc. Thus, the input energy per unit area E_{IP}/A at a base layer during the earthquake may be readily computed for engineering purposes if the earthquake magnitude and the focal distance are given.

By subtracting the energy E_d, that is reflected downward into the base layer due to the impedance contrast at the layer boundary, from the input energy E_{IP}, the earthquake energy E_{EQ}, that is transmitted into the upper layer, can be computed (i.e., E_{EQ} = E_{IP} - E_d). Assuming that all the energy E_{EQ} transmitting into the upper layer is absorbed by the upper layer due to the slope failure as observed in the shake table model tests, the energy ratio E_{EQ}/E_{IP} can be formulated as (Kokusho et al. 2007):

$$E_{EQ}/E_{IP} = 4\alpha/(1+\alpha)^2 \qquad (12)$$

where α is the impedance ratio of the sloping upper layer to the base layer. A small portion out of the energy transmitted into the upper layer (E_{EQ}) may be dissipated by cyclic straining of soil or internal soil damping. If this portion is denoted as E'_{EQ}, the

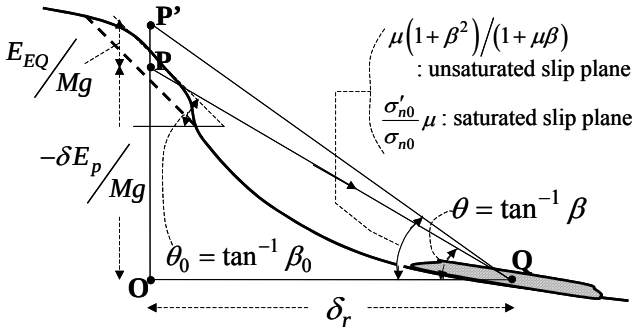

Fig. 8. Graphical evaluation method for run-out distance of seismically induced slope failure.

energy causing the slope failure is ($E_{EQ} - E'_{EQ}$). Hence, if E'_{EQ} is not negligibly small, then E_{EQ} in Eqs.(8) and (8') should be replaced by ($E_{EQ} - E'_{EQ}$).

The sliding soil mass M in Eqs.(8) and (8') may be determined by conventional slip surface analyses, where a potential slip surface having the lowest factor of safety is found. However, in failures of natural slopes such as those during the 2004 Chuetsu earthquake, the potential slip surface may be reasonably assumed to coincide with a bedding plane or a weak seam observed in site investigations.

In the above considerations, the slope was idealized to be straight. However, for slopes that are not straight as illustrated in Fig. 8, Eqs.(1)-(8') can still be used if β is taken as a global inclination of a straight line PQ (directly connecting the centroids of a failed soil mass before and after failure) different from the initial inclination β_0 , and μ as the average mobilized friction coefficient over the travel distance. Let us assume in Fig. 8 that the center of gravity of the sliding soil mass moves from P to Q during failure. The drop height PO ($-\delta E_p / Mg$) divided by the horizontal displacement OQ (δ_r) corresponds to the global inclination β of the slope from Eq.(4), hence,

$$\frac{-\delta E_p / Mg}{\delta_r} = \beta \qquad (13)$$

On account of the earthquake energy, the centroid can be considered to rise up by E_{EQ}/Mg , from P to P'. The inclination of the line P'Q, or the ratio of the height P'O expressed as $\left(-\delta E_p / Mg + E_{EQ} / Mg\right)$ to the horizontal displacement (δ_r), OQ, can be expressed using Eqs.(4) and (6) as

$$\frac{-\delta E_p / Mg + E_{EQ} / Mg}{\delta_r} = \mu \frac{1+\beta^2}{1+\mu\beta} \qquad (14)$$

For cases of saturated slip plane, the inclination of the line P'Q can be expressed from Eqs.(4) and (6') as:

$$\frac{-\delta E_p / Mg + E_{EQ} / Mg}{\delta_r} = \frac{\left(\mu\sigma'_{n0} - \beta\sigma_{n0}\right)}{\sigma_{n0}} + \beta = \mu\left(\sigma'_{n0}/\sigma_{n0}\right) \qquad (15)$$

Consequently, the procedure for run-out distance evaluation is:

1) Determine the dimension and weight of a potential sliding soil mass and its centroid P.
2) Determine the mobilized friction coefficient μ .
3) Evaluate the earthquake energy E_{EQ} by Eqs.(10)-(12).
4) Locate Point P', which is by E_{EQ}/Mg higher than P or by $\left(E_{EQ} - E'_{EQ}\right)/Mg$ higher if E'_{EQ} is not negligibly small.
5) Starting at Point P', draw a line having an inclination of $\mu\left(1+\beta^2\right)/\left(1+\mu\beta\right)$ or $\left(\sigma'_{n0}/\sigma_{n0}\right)\mu$ for a unsaturated or saturated condition, respectively, until it intercepts the slope surface (Point Q). Then from the geometry of the slope, δ_r can readily be obtained.

This very simple procedure can be conveniently used to evaluate the run-out distance for seismically induced slope failure for developing slope failure hazard maps in zonation studies.

SLOPE FAILURES DURING RECENT EARTHQUAKES

In using the energy approach, it is very important that the mobilized friction coefficient μ be properly determined in advance. It may be possible in some cases to evaluate it directly from soil tests sampled from specific sites. However, due to complexity of actual slope failures in the field, a more robust

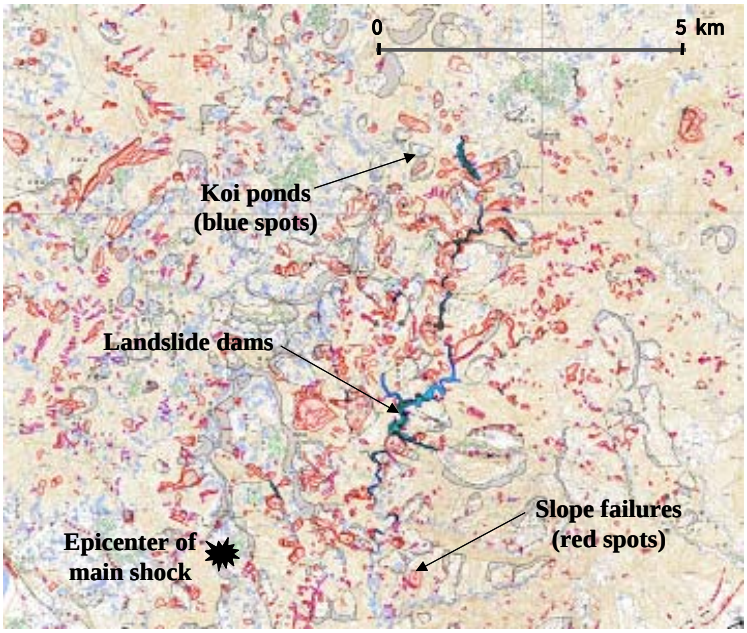

Fig. 9. Center part of the damaged area with countless slope failures, Koi-ponds and landslide dams

method is to accumulate as many case studies as possible and back-calculate the friction coefficients. The obtained values will depend on various site conditions such as topography, geology, mechanical properties, water content, etc. Recent strong earthquakes provide us with a rare opportunity to evaluate the mobilized friction coefficients using this method.

2004 Niigata-ken Chuetsu earthquake

During the Niigata-ken Chuetsu earthquake of October 23 (M_J=6.8, thrust fault, focal depth 13 km), 2004, more than 4000 slope failures occurred as a result of the main shock and several strong aftershocks 200 km north of Tokyo in the main island of Japan. The damaged area shown I Fig. 9 was known as a landslide-prone area of green-tuff, with geological structures of active folding. Slopes were composed of weak sedimented rock of Neogene, interbedding layers of strongly weathered sandstones and mudstones, and bedding planes had a strong effect on the slope failures. A number of red spots in Fig. 9 indicate slope failures, some of which blocked streams making landslide dams. Countless blue spots also shown in the figure represent Koi ponds constructed on mountain slopes by farmers, because Koi cultivation has long been an important local industry in this region from old times.

The slope failures due to this particular earthquake may be classified into 3 types, as illustrated in Fig. 10:

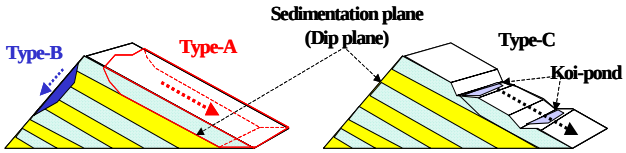

Fig. 10. 3 types of slope failures, A, B, and C, occurred during 2004 Niigataken Chuetsu Earthquake.

Fig. 11. Higashi-Takezawa slide (Type-A) seen from top of scarp (Large soil mass slid down as a block along the arrows, filled the valley, climbed up to the other side, and dammed the river).

- Type-A: Deep slips parallel to sedimentation planes (dip plane), in gentle slopes of around 20 degrees. In many cases, displaced soil mass had originally been destabilized by river erosion or road construction, and glided as a rigid body along a slip plane on mudstone. Displaced soil volume was very large and the translating soil block sometimes showed little surface disturbance.
- Type-B: Shallow slips of 1 - 2 m deep not parallel to sedimentation planes in slopes steeper than 30 degrees). These failures far outnumbered the Type-A failures, but the individual soil volume was not very large. Soils ran out as pieces, sometimes leaving trees with deep roots in their original locations.
- Type-C: Slope failures in highly weathered colluvial soils in places where Koi-ponds and terraced paddy fields were located. Though this type was similar to Type-A, involving an underlying dip slip plane of mudstone, the displaced soil mass was highly weathered because of repetitive slope failures in the past and developed into a mud flow with long travel distance. This type of failure seems to be unique to this region because of the countless Koi-ponds located in the damaged area. The failure was obviously associated with the ponds in causing overflow by seiche during shaking and also subsequent piping through induced cracks, leading to delayed flow-type failure of the colluvial soils.

In most of the slope failures, sandstones were largely responsible mainly because of their weakness due to strong weathering. The unconfined compression strengths of intact sandstones were smaller than q_u=200 kPa, considerably weaker than those of inter-bedded mudstones of q_u ≈800 kPa. Also noted is that the sandstones consisting of poorly graded fine particles had higher permeability of the order of 10^{-3} cm/s than that of mudstones of the order of 10^{-4}-10^{-6} cm/s and hence may have served as aquifer (Kokusho et al. 2009b).

The most representative example of failure Type-A is shown in Fig. 11 (Higashi-Takezawa), where highly weathered sandstone (actually dense sandy soil), 15 m thick, slid about 100 meters along an underlying mudstone slip plane of 20 degrees. The displaced soil mass dammed a river, making a natural reservoir on the right side of the photograph.One of the largest Type-B failures is shown in Fig. 12 (Haguro Tunnel Entrance) where about 80 thousands m^3 of soil debris ran out more than 100 m. Soil mass of 4 – 8 m thick, disintegrated into small pieces, slid down the slope steeper than 35 ° and attacked houses below.

Fig. 13 shows a typical slope failure of Type-C (Mushikame), where about 160 thousands m^3 of soil with high water content ran down more than 100 m into a river below as a mud flow. The Koi pond seems to have played an important role in triggering the failure because it kept soil water content high making the slope seismically instable, and internal erosion by pond water eventually

Fig. 12 Photograph of Haguro Tunnel Entrance slide (Type-B) where surface shallow soil slid down and disintegrated into pieces.

Fig. 13 Photograph of Musikame slide (Type-C) where a Koi-pond triggered long runout distance failure (after http://www:ajiko.co.jp)

Fig. 14 Photograph of Aratozawa huge landslide (Type-A) during 2008 Iwate-Miyagi Inland earthquake.

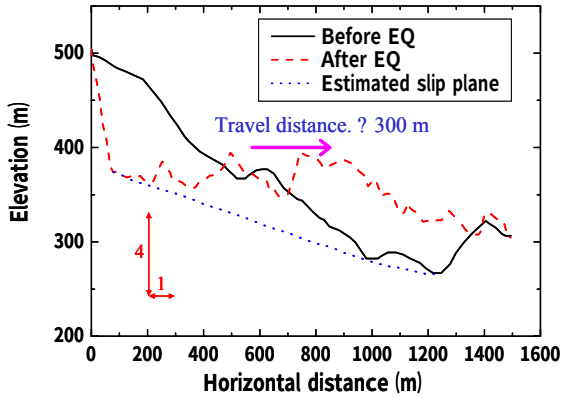

Fig. 15 Cross-sectional view of Aratozawa landslide along the centerline shown in Fig.14.

caused large-volume failures. However, a lot still needs to be learned before the exact mechanism of the Type-C failure is fully understood.

2008 Iwate-Miyagi Inland Earthquake

Iwate-Miyagi Inland earthquake occurred in June 14, 2008, 400 km north of Tokyo in the main island of Japan. During the earthquake (M_J=7.2, thrust fault, focal depth 8 km), very strong ground motions were measured in the near fault zone of PGA of 1G–2G PGV of more than 50 cm/s. About 1900 slope failures occurred there, the geology of which was mostly of volcanic rock of Miocene and Pliocene, welded/non-welded tuff, sandstone, silty stone, etc.

Fig. 14 shows the largest slope failure in Aratozawa, where the area of 1.2 km by 0.8 m next to a man-made reservoir slid almost horizontally more than 300 m along a deep-seated slip plane. The total volume may be evaluated as 35-70x10^6 m^3. The cross-sectional view along the center line is shown in Fig.15. Though the exact location of the major slip plane is difficult to demonstrate, it is assumed as drawn in the dashed line, with a dip angle of less than 5 degrees. The sliding direction was slightly skewed from the direction toward the reservoir. The sliding debris collided with a mountain in front filling a valley in between and also rushed into the reservoir triggering small tsunami. This slide may also be classified as Type-A of rigid body movement along the deep slip surface which was probably saturated and under high water pressure, though independent movements from part to part along minor shallower slip planes presumably diverting from the major one were also apparent.

RUNOUT DISTANCE AND FRICTION COEFFICIENT

For a number of slope failures in the damaged area during the 2004 earthquake, the ground surface elevations before and after the earthquake were compared to quantify the 3-dimensional topographical changes. The post-earthquake elevation was obtained by DEM (Digital Elevation Map) data based on air-born laser survey carried out 5 days after the earthquake. Due to the absence of corresponding data just before the earthquake, air-photographs taken in 1975 and 1976 were used to develop the pre-earthquake DEM by manual reading. The maximum potential error involved in the post-earthquake elevations was ± 0.5 m, while that of pre-earthquake elevations was ± 1.0 m. Some of digitized DEM data are available in a separate literature (Kokusho et al. 2009b). For the 2008 earthquake, the topographic changes investigated by Tohoku Forestry Agency (www.rinya.maff.go.jp/tohoku/) was used.

Cross-sectional change of failed slopes was developed from the DEM data before and after the earthquake. The slip surface which cannot directly detected from DEM was determined reliably from the exposed scarp or slip plane in the upslope side, from the original location of the valley in the downslope side and from the global change of slope configuration. The followings are some preliminary findings thus obtained on the runout distance of the failed slopes.

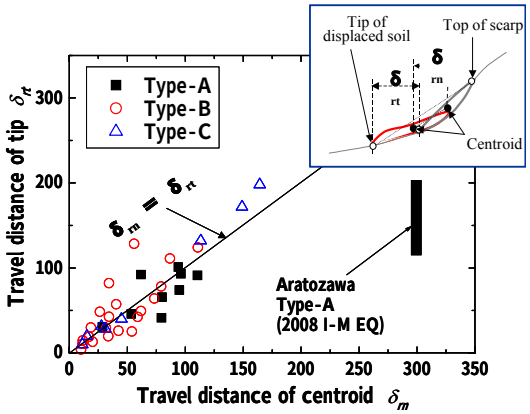

Fig. 16 Runout distances for centroid δ_{rn} and for tip δ_{rt} of displaced soil mass in failed slopes during the earthquake.

From the viewpoint of disaster mitigations, the run-out distance for tips of displaced soil mass δ_{rt} is more important than that of the centroids, δ_{rn} as illustrated in Fig. 16. Hence, the two values were read off from the 3-dimensional changes of failed slopes and plotted in the horizontal and vertical axes respectively in Fig. 16. No big difference between them can be observed except the 2008 Aratozawa slide because the plots spread out almost randomly along the line, $\delta_{rt} = \delta_{rn}$, although δ_{rt} is slightly larger than δ_{rn} for Type-C failures of longer runout distance in particular, indicating that the value δ_{rn} may be used as a representative travel distance.

In Fig. 17, the initial slope gradient β_0 is correlated with the runout distance δ_{rn}. Here the value β_0 was approximated as a gradient of the line connecting the highest and lowest surface elevations of the failed mass in its initial condition. The data points, despite the significant dispersions, indicate an unexpected trend so that the runout distance clearly increases with decreasing β_0 not only individually, as approximated by the β_0 versus δ_{rn} curves for Types-A, B and C respectively, but also as a whole.

In Fig. 18, the runout distance δ_{rn} is correlated with the logarithm of the failed soil volume V_f, which obviously shows the increase of δ_{rn} with increasing V_f as a whole, though the trend is different depending on the failure types. Note both in Figs. 17 and 18, that the distance δ_{rn} for Type-C is evidently larger than other types in long travel-distance failures presumably on account of higher water content of soil debris.

The input energy, E_{IP}, during the 2004 earthquake at the base layer of the slopes was evaluated from several KiK-net vertical array records around the area (Kokusho et al. 2009b). In Fig. 7, incident energies per unit area E_{IP}/A for this particular

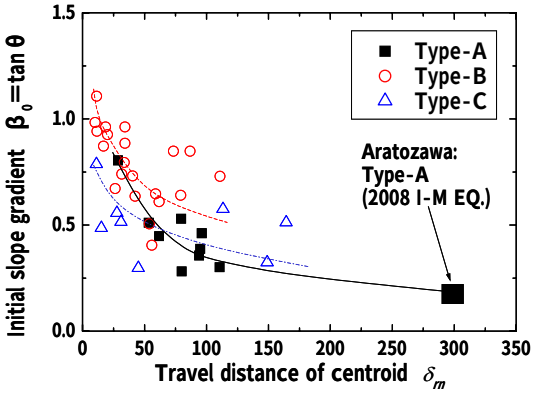

Fig. 17 Initial slope gradient of failed soil mass β_0 plotted versus runout distance δ_{rn} for 3 types of failures.

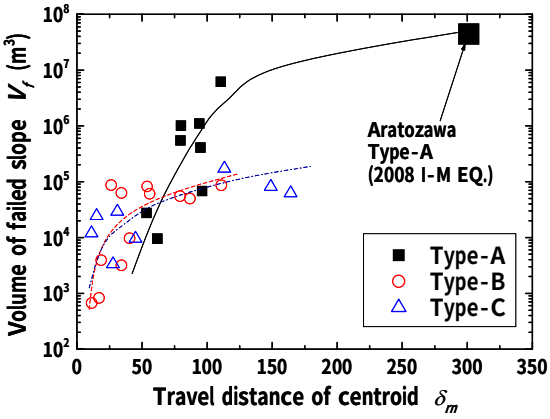

Fig. 18 Volume of failed soil mass V_f plotted versus runout distance δ_{rn} for 3 types of failures.

earthquake are plotted with solid circles. The plots may be approximated by Eq.(10) with the value E_0 calculated by Eq.(11) assuming M=6.7 to have better matching than M=6.8. Fig. 19 depicts the 2-dimensional distribution of the input energy per unit area E_{IP}/A for the earthquake thus calculated for all the locations of identified slope failures in the damaged area (Kokusho et al. 2009b) during the 2004 earthquake. The corresponding energy for the Aratozawa slide during the 2008 earthquake was evaluated from Eqs.(10) and (11) as 1530 kJ/m^2, much larger than the other cases because the earthquake magnitude was larger (M_J7.2) and the site was very near from the epicenter.

Then, the maximum earthquake energy E_{EQ}/A to be used for each slope failure was calculated from Eq.(12) for this particular earthquake as E_{EQ}/E_{IP} =0.71 assuming the impedance ratio between sloping surface layers and base layers as α =0.3 (Kokusho and Ishizawa 2009). The internally dissipated energy E'_{EQ} by liquefaction or soil damping was assumed to be negligibly small compared to other energies and the total density of the soil, ρ_t, was approximated as 1.8 t/m^3 (Kokusho et al. 2009b).

With all preparations mentioned above, mobilized friction coefficients were calculated by Eq.(8') for a number of slope failures during the 2004 Chuetsu earthquake and the 2008 Aratozawa slide. Fig. 20 shows typical examples how the failed soil volume was idealized by a rectangular block. Thus, the horizontal dimension of the soil block and its thickness before and after the failure, the initial slope inclination β_0, the horizontal displacements of the centroid δ_{rn} and the global inclination of the line β connecting the centroid of the block before and after the failure were quantified based on the DEM data.

It is not easy to exactly grasp the ground water conditions during the 2004 earthquake in a number of failed slopes studied here. There was heavy precipitation before the 2004 earthquake (Kokusho et al. 2009b) and it may well be judged that the slip planes in Type-A and C failures were saturated at the time of earthquake because they passed through highly permeable weathered sandstone layers immediately above low-permeability mudstones. Water was actually running on slip planes of mudstones several days to a few weeks after the 2004 earthquake, while the upper soil mass was mostly unsaturated. Also taken into account was that permeable sandstone and impermeable mudstone was essentially interbedded, which interrupted a formation of vertically thick continuous aquifer. Hence, Eq.(8') was used for all slope failures taking $\sigma'_{n0} \approx \sigma_{n0}$ to back-calculate the mobilized

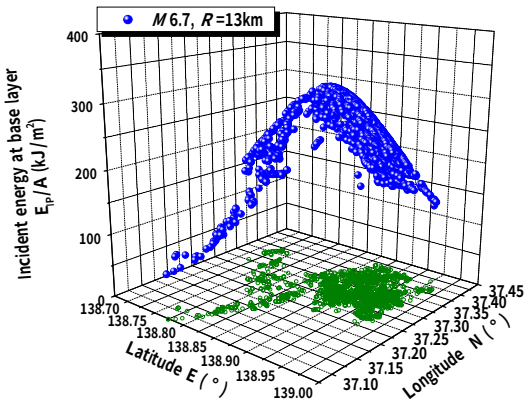

Fig. 19 Input energy per unit area E_{IP}/A for the main shock calculated for all slope failures in the area to be used in back-calculation of friction coefficients.

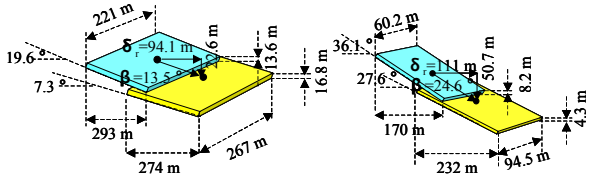

(a) Higashi-Takezawa (Type-A)

(b) Haguro Tunnel Entrance (Type-B)

Fig. 20 Simplified rigid block models for representative slope failures.

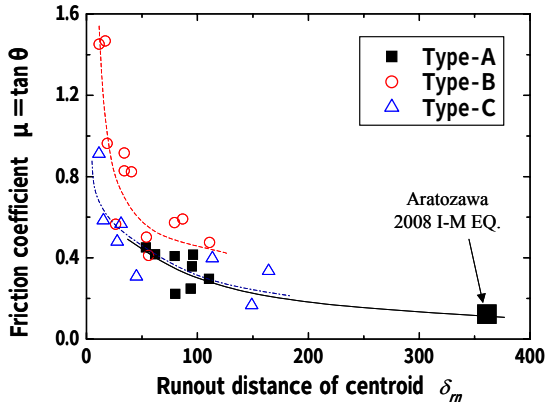

Fig. 21. Friction coefficient μ versus runout distance δ_{rn} for 3 types of failures.

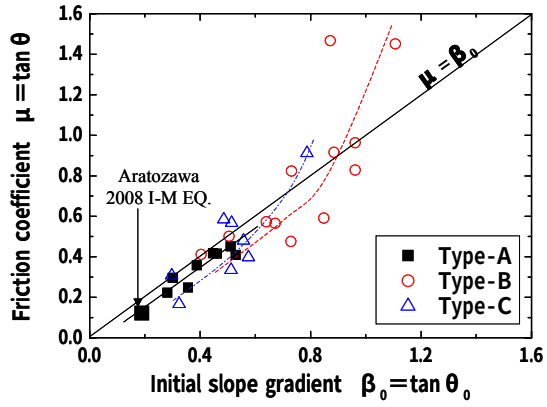

Fig. 22. Friction coefficients μ versus initial slope gradient β_0 for 3 types of failures.

friction coefficient $\mu = \tan\phi$ from the solid block models exemplified in Fig. 20. More detailed discussion on the effect of uncertainties in the ground water condition is available in another literature (Kokusho and Ishizawa 2009).

Fig. 21 shows the plots of the back-calculated friction coefficients μ versus the runout distance of the centroid δ_{rn} for a number of slopes investigated here in detail. They are classified into Type-A, B and C in accordance to the characteristics previously mentioned and their plots are approximated by the curves. The μ-value tends to increase with decreasing runout distance for all the failure types. The increasing rate of μ becomes high for δ_{rn} < 40-50 m while μ tends to be stable for δ_{rn} larger than that. For the same runout distance, the μ –value of Type-B failures seems to be larger than that of Type-A or C probably because the slip plane is crossing the dip plane.

In Fig. 22 the back-calculated friction coefficients, μ, are plotted versus initial slope gradients, β_0. Note that, for smaller values of β_0 corresponding to Type-A or C, most of the back-calculated μ-values are lower than or almost identical to the diagonal line of $\mu = \beta_0$, indicating that the friction coefficients μ, which, needless to say, were originally larger than β_0, decreased due to the effect of earthquake shaking and subsequent sliding. The μ-value smaller than β_0 implies that the failed soil mass accelerates first and then decelerates due to gentler or reverse slope angles in down-slope sections. This was presumably what happened in Higashi-Takezawa, where the friction coefficient μ =tan13.5º =0.248 (considerably smaller than β_0 =tan19.6º =0.356 as shown in Fig. 20(a)) allowed the failed soil mass to accelerate and climb up the opposite side of the valley, as shown in the photograph in Fig. 11. In contrast, the data points with higher values of β_0 (most of them belong to Type-B) are plotted on both sides of the diagonal line $\mu = \beta_0$. They tend to jump up crossing the line with increasing μ as approximated by the curves in Fig. 22 despite large data scatters.

The exact mechanism how the friction coefficient lower than the initial slope gradient was realized is yet to be clarified. In Type-A in particular, seismically induced pore-pressure buildup or liquefaction in highly weathered sandstone near the slip plane seems to have occurred. In Type-C failures, the high water content may have transitioned soil debris into high-speed mudflows due to pore-pressure build-up.

It should also be noted in Fig. 22 that the mobilized friction coefficient back-calculated from the case studies are highly dependent on the initial slope gradient. It is quite different from man-made slopes in which strength parameters are normally considered to be independent of a slope gradient. This may indicate that the friction coefficients of natural slopes strongly reflect their long-time exposures to previous natural loads; namely, steeper slopes are sustained there because they survived previous seismic and rainfall events on account of their higher mobilized friction coefficients.

In Fig. 23, the same back-calculated μ-values are plotted again versus the volumes of failed slopes on the semi-logarithmic diagram. Despite large scatters in the data, a clear decreasing trend of μ can be seen as the volume V_f increases from 10^3 to 10^7 m^3 irrespective of the failure types, though the volume-dependency is more pronounced in Type-B failures.

As previously explained, the ratio between the earthquake energy for slope failure E_{EQ} and the potential energy $-\delta E_p$ can be expressed by Eqs.(7) or (7'). In Fig. 24, the energy ratios $-\delta E_p / E_{EQ}$ evaluated by Eq.(7') ,assuming saturated slip planes, are taken versus the volumes of failed slopes V_f on the full logarithmic diagram. It is remarkable that, for all the slope failures of their volumes larger than 10^3 m^3, the value $-\delta E_p / E_{EQ}$ is larger than unity, and for those larger than 10^5 m^3, it is as large as several tens. This indicates that the thicker the failed slope and the higher its drop height, the smaller the contribution of the earthquake energy compared to the potential energy, as already pointed out theoretically (Kokusho and Ishizawa 2007). This finding also indicates that accuracy in determining the energy E_{EQ} may not be so critical for the large volume failures.

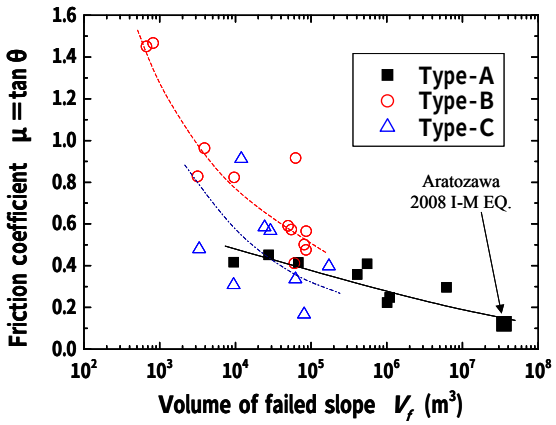

Fig. 23. Friction coefficients μ versus failed soil volume V_f for 3 types of failures.

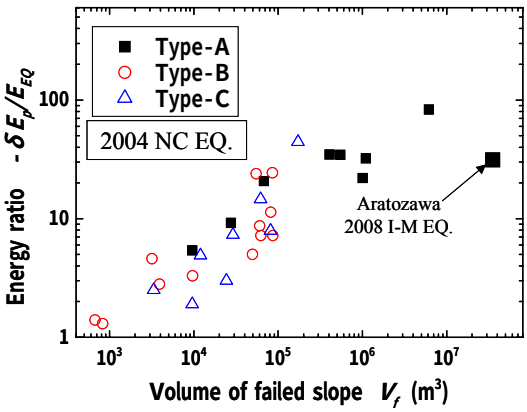

Fig. 24. Energy ratio $-\delta E_p / E_{EQ}$ versus failed soil volume V_f for 3 types of failures.

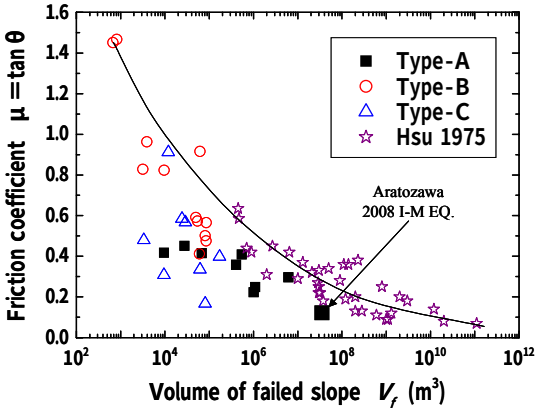

Fig. 25. Friction coefficients μ versus failed soil volume V_f obtained in this research, compared with analogous relationship for huge landslides published by Hsu(1975).

However, the contribution of earthquake energy seems still important not directly by supplying the driving energy but more indirectly by reducing friction coefficient μ through dynamic/cyclic loading. There are possibilities that some of the slope failures of Type-A or C in particular may have occurred after the end of earthquake shaking. In such cases the direct contribution of earthquake energy should be omitted in the discussions above. The discussion on this effect is available in Kokusho et al. (2009a).

A relationship similar to Fig. 23 between the friction coefficients μ and the volume of failed slope V_f had been presented based on case histories of huge landslides not necessarily associated with earthquakes by Hsu 1975. Fig. 25 illustrates the superposition of the two research results. Unlike this research, the friction coefficient μ in the Hsu's paper was defined in a different manner as the gradient of a line connecting the top of the scarp and the tip of the displaced mass, though it normally gives a similar gradient to that connecting the centroids (the global inclination β) as inferred from the illustration in Fig. 16. Fig. 25 shows a remarkable compatibility in the data points of the two researches in the wide range for the failed soil volume of 10^3-10^{11} m^3 particularly for the Type-B failures. For the Type-A and C failures, the data points are slightly lower than the global approximation curve in Fig. 25, presumably due to the effect of dip slip planes and large involvement of water, respectively.

Thus, the back-calculated friction coefficients are found to have clear dependency on slope inclination, failed soil volume, dip plane and water content. Some of these findings, though more or less affected by specific site conditions, may possibly hold in slope failures in general and serve as a basis in determining the friction coefficients in slope failure predictions. More case studies for other earthquake-triggered landslides are certainly needed to increase the applicability of the back-calculated results to generic site conditions.

CONCLUSIONS

An energy approach for slope failure evaluation has been developed by first conducting a series of innovative shake table model tests of dry sand slopes and then examining the associated energy balance by comparing with a Newmark-type rigid block model, which has clarified the followings.

1) In shake table tests of dry sand slopes with different slope inclinations and different input frequencies, the earthquake energy E_{EQ} to be directed to slope failure can be successfully measured, quantifying the energy balance involved in the failure of the model slopes.
2) The model tests yields a unique relationship between the energy E_{EQ} and residual slope displacement δ_r for each slope inclination which is independent of input frequency. This relationship also shows a clear threshold of E_{EQ} below that δ_r=0, which are again independent of input frequency, implying that not only the residual displacement but also the initiation of slope failure may be determined uniquely by the energy. In contrast, acceleration cannot uniquely determine not only the displacement but also the initiation of the failure.
3) Comparison of the test results with the energy balance in a Newmark-type rigid block model indicates that the model, which apparently possesses a different failure mechanism, can almost perfectly emulate a continuously deforming sand slope, provided that an appropriate friction coefficient μ can be estimated.
4) A simple graphical procedure is proposed to evaluate the run-out distance of seismically induced slope failures for developing hazard maps from earthquake energy E_{EQ} and the mobilized friction coefficient μ, once an instable soil mass is detected. The energy E_{EQ} may be determined from the input seismic wave energy, E_{IP}, which can be readily computed from a given earthquake magnitude M and focal distance R without using ground motion time histories.

From case studies of a number of slope failures during the 2004 Niigataken Chuetsu earthquake and Aratozawa huge slide during 2008 Iwate-Miyagi earthquake, the followings have been revealed;

5) Slope failures in the earthquake may be classified into 3 types, A, B and C, considering the dominant effect of dip planes and high water content in debris.
6) The displacement of the centroid may be used as a representative travel distance of failed slopes because, in most cases, it does not differ so much from that of the tip of failed soil mass.
7) Quite unexpectedly, the debris travel distance tends to increase with decreasing initial slope gradient. The distance also tends to increase with increasing volume of the displaced soil. These trends are essentially the same, though slightly different depending on the failure types.

The energy approach applied to the slope failures to back-calculate the mobilized friction coefficients exhibited during the earthquakes has unveiled the following major findings.

8) The back-calculated friction coefficients μ are highly dependent on the initial slope gradient β_0 and increases with increasing gradient. This is quite different from man-made banking slopes in which μ is considered independent of β_0.
11) For lower β_0, the back-calculated μ-values are lower than the line $\mu = \beta_0$, indicating that μ, originally larger than β_0, decreases after the shaking. Also indicated is that the failed soil mass accelerated first and then decelerated due to gentler or reverse slope angles in down-slope sections. In contrast, for higher values of β_0, the μ-value tends to be higher than the diagonal line.
12) For slope failures of large volumes, the energy ratio $-\delta E_p / E_{EQ}$ is several tens, indicating small contribution of the earthquake energy E_{EQ} compared to the potential energy $-\delta E_p$. However, the earthquake energy still plays an important role as a trigger of the failure by changing soil properties rather than directly by driving the soil mass.
13) A clear decreasing trend of μ can be recognized as the failed soil volume increases from 10^3 to 10^7 m^3 irrespective of the failure types. The decreasing trend in this research is compatible with that presented in previous case studies on huge landslides.

ACKNOWLEDGEMENTS

A part of this research was supported by Special Coordination Funds for Promoting Science and Technology, "Earthquake damage in active folding areas -Creation of a comprehensive data archive and suggestions for its application to remedial measures for civil-infrastructure systems-" of Japan Science & Technology Agency. Mr. Kyosuke Nishida and other students in Graduate and Undergraduate Course of Civil Engineering Department, Chuo University, who contributed in promoting this research for several years, are gratefully acknowledged. NIED (National Research Institute for Earth Science and Disaster Prevention) in Tsukuba, Japan who recorded and electronically publicized KiK-net data used in the research is gratefully appreciated.

REFERENCES

Gutenberg, B. [1955], "The energy of earthquakes", *Quarterly Journal of the Geological Society of London*, Vol.CXII, No.455, 1-14.

Hsu. J. [1975], "Catastrophic debris streams generated by rockfalls" *Geological Society of America Bulletin*, v.86, Doc.no.50117, p.129-140.

Kokusho, T, and K. Kabasawa, K. [2003], "Energy approach to flow failure and its application to flow due to water film in liquefied deposits", Proc. of International Conference on Fast Slope Movements, Prediction and Prevention for Risk Mitigation, Naples, 297-302.

Kokusho, T. and Ishizawa, T. [2007], "Energy approach to earthquake-induced slope failures and its implications", *Journal of Geotechnical and Geoenvironmental Engineering*, ASCE, Vol.133, No.7, 828-840.

Kokusho, T., Motoyama, R. and Motoyama, H. [2007], "Wave energy in surface layers for energy-based damage evaluation", *Soil Dynamics & Earthquake Engineering*, 27, Elsevier, 354-366.

Kokusho, T., Ishizawa, T. and Nishida, K. [2009a], "Travel distance of failed slopes during 2004 Chuetsu earthquake and its evaluation in terms of energy", *Soil Dynamics & Earthquake Engineering*, *Elsevier*, 29, 1159-1169.

Kokusho, T., Ishizawa, T. and Hara, T. [2009b], "Slope failures during the 2004 Niigataken Chetsu earthquake in Japan", *Earthquake Geotechnical Case Histories for Performance-Based Design,* Balkema, CRC Press, 47-70.

Kokusho, T. [2009], "PBD in earthquake geotechnical engineering and energy-based design, Special Discussion Session –Future directions of performance-based design-", *Performance-Based Design in Earthquake Geotechnical Engineering – from Case History to Practice, Proceedings of the International Conference on Performance Based Design in Earthquake Geotechnical Engineering (IS-Tokyo 2009)*, Balkema, CRC Press, 359-362.

Makdisi, F. I. and Seed H. B. [1978], "Simplified procedure for estimating dam and embankment earthquake –induced deformations", *Journal of Geotechnical Engineering*, Div. ASCE, Vol.104, No.GT7, 849-867.

Newmark, N. M. [1965], "Effects of earthquakes on dams and embankments", Fifth Rankine Lecture, *Geotechnique* Vol.15, pp.139-159.